JOURNAL OF COMPUTATIONAL PHYSICS 48, 441–461 (1982)

Application of Multigrid Methods for Integral Equations to Two Problems from Fluid Dynamics

H. SCHIPPERS

Mathematisch Centrum, 1009 AB Amsterdam, The Netherlands

Received January 13, 1982

Multigrid methods are applied in order to solve efficiently the nonsparse systems of equations that occur in the numerical solution of the following problems from fluid dynamics: (1) calculation of potential flow around bodies and (2) calculation of oscillating disk flow. Problem (1) is reformulated as a boundary integral equation of the second kind that is approximated by a first-order panel method resulting in a full system of equations. This method is in widespread use for aerodynamic computations. The second problem is described by the Navier–Stokes and continuity equations. By means of the von Kármán similarity transformations these equations are reduced to a nonlinear system of parabolic equations which are approximated by implicit finite difference techniques. From the periodic conditions in time one obtains a nonsparse system of equations. For these two problems from fluid dynamics the fast convergence of multigrid methods for integral equations is established by numerical experiments.

INTRODUCTION

Multigrid methods have been advocated by Brandt [1] for solving sparse systems of equations that arise from discretization of partial differential equations. Convergence and computational complexity of such multigrid techniques have been studied since. In [2] we have shown that these techniques can also be used advantageously for the nonsparse systems that occur in the numerical solution of Fredholm integral equations of the second kind

$$f = Kf + g, \tag{1}$$

where g belongs to a Banach space X and the integral operator K is compact on X. Theoretical and numerical investigations show that multigrid methods give the solution of (1) in $O(N^2)$ operations as $N \to \infty$, whereas other iterative schemes take $O(N^2 \log N)$ operations (where N is the dimension of the finest grid). In practice this results in algorihtms for the solution of these integral equations that are significantly more efficient than the other schemes. In the present paper we apply multigrid methods to the following problems from fluid dynamics.

0021-9991/82/120441-21$02.00/0

Calculation of Potential Flow around Bodies

The total velocity potential ϕ is assumed to be the superposition of the potential ϕ_∞, due to a uniform onset flow and a perturbation potential ϕ_d, due to a doublet distribution at the body surface. This approach leads to a Fredholm equation of the second kind for the unknown doublet distribution. We introduce a multigrid method which makes use of a sequence of grids that are generated by dividing the body surface into an increasing number of smaller and smaller panels. On these grids the doublet distribution is assumed to be constant over each panel. For a two-dimensional (2-D) aerofoil we have applied the multigrid method to the calculation of circulatory flow around Kármán–Trefftz aerofoils. The use of multigrid techniques becomes more preferable for 3-D problems because the number of panels is much larger than for 2-D ones. The calculations have been performed for the flow around an ellipsoid. From numerical investigations it follows that ± 3 multigrid cycles are sufficient to obtain the approximate solution.

Calculation of Oscillating Disk Flow

This application deals with the rotating flow due to an oscillating disk at an angular velocity $\Omega \sin \omega\tau$. The Navier–Stokes and continuity equations are reduced by means of the von Kármán similarity transformations to

$$(\omega/\Omega) f_t = (\Omega/2\omega) f_{zz} + 2hf_z - f^2 + g^2, \tag{2}$$

$$(\omega/\Omega)\, g_t = (\Omega/2\omega)\, g_{zz} + 2hg_z - 2fg, \tag{3}$$

$$h_z = f, \tag{4}$$

where (f, g, h) is a measure of the velocity vector in a cylindrical polar coordinate system (r, ϕ, z). For a single disk problem the boundary conditions are

$$f = h = 0, \qquad g = \sin t \quad \text{at } z = 0; \qquad f = g = 0 \quad \text{for } z \to \infty. \tag{5}$$

In [3] the author has shown that the periodic solution

$$h(z, 0) = h(z, 2\pi), \qquad g(z, 0) = g(z, 2\pi) \tag{6}$$

can be obtained by implicit finite difference schemes taking the state of rest as an initial condition. The transient effects have been eliminated by calculating a sufficiently large number of periods. Using the multigrid method we do not simulate the physical process, but reformulate problem (2)–(6) as

$$(f, g, h) = K(f, g, h), \tag{7}$$

where K is a nonlinear integral operator. The multigrid method for integral equations is used to solve (7). For $\Omega = 0.1\omega$ the computational work has been reduced by a factor of 10.

Calculation of Potential Flow around Bodies

For potential flow around a 2- or 3-D body there exists a velocity potential ϕ satisfying Laplace's equation

$$\Delta\phi = 0 \tag{8}$$

with boundary conditions,

$$\frac{\partial\phi}{\partial n_e} = 0 \qquad \text{along the boundary } S, \tag{9}$$

where $\partial/\partial n_e$ denotes differentiation in the direction of the outward normal to S and

$$\phi(\zeta) \to \phi_\infty(\zeta) \qquad \text{for} \quad |\zeta| \to \infty, \tag{10}$$

with ϕ_∞ the velocity potential due to a uniform onset flow. If the flow is noncirculatory, we have $\phi_\infty(\zeta) = \mathscr{V} \cdot \zeta$, with $\mathscr{V}$ the velocity vector of the undisturbed flow. Here $\mathscr{V} \cdot \zeta$ denotes the usual inner product in $\mathbb{R}^2$ or in $\mathbb{R}^3$. We represent the velocity potential ϕ as

$$\phi(\zeta) = \phi_\infty(\zeta) + \phi_d(\zeta),$$

with ϕ_d the double layer potential given by

$$\phi_d(\zeta) = \frac{2^{1-m}}{\pi} \int_S \mu(x) \frac{\cos(n_x,\ x-\zeta)}{|x-\zeta|^{m-1}}\, dS_x, \qquad \zeta \notin S, \tag{11}$$

where $m = 2, 3$ for the 2- and 3-D case, respectively, and n_x is the outward normal to the boundary S at the point x. The doublet distribution μ is such that ϕ satisfies the boundary condition

$$\phi^-(\zeta) = 0, \tag{12}$$

where ϕ^- denotes the limit from the inner side to S. Using the Plemelj–Privalov formulae (see [4]) we obtain the following integral equation:

$$\mu(\zeta) + \frac{2^{2-m}}{\pi} \int_S \mu(x) \frac{\cos(n_x,\ x-\zeta)}{|x-\zeta|^{m-1}}\, dS_x = -2\phi_\infty(\zeta), \qquad \zeta \in S. \tag{13}$$

Assuming the boundary S to be sufficiently smooth, it can be proven that the solution of interior Dirichlet problem (12) also satisfies Neumann problem (8)–(10) for the exterior of the boundary S.

Calculation of Circulatory Flow around an Aerofoil

For circulatory flow around an aerofoil one must introduce a cut to make the velocity potential single valued. The Kutta condition of smooth flow at the trailing

edge can be satisfied if we construct the cut from the trailing edge to infinity. We denote the upper and lower side of the cut by S^+ and S^-, respectively. The contour composed of the aerofoil S and the cut is denoted by $S^- + S + S^+$. Along the cut there exists a constant discontinuity in velocity potential. The jump is represented by a constant double layer potential with strength μ^+ and μ^- along S^+ and S^-, respectively. The difference $\mu^- - \mu^+$ is equal to the circulation which is taken positive in clockwise direction.

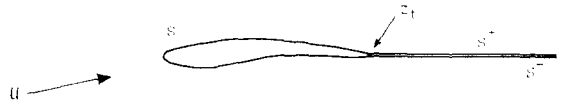

We can represent the velocity potential by

$$\phi(\zeta) = \mathscr{U} \cdot \zeta + \frac{1}{2\pi} \int_{S^- + S + S^+} \mu(x) \frac{\cos(n_x, x - \zeta)}{|x - \zeta|} dS$$

or rewritten

$$\phi(\zeta) = \mathscr{U} \cdot \zeta + \phi_d(\zeta) + (1/2\pi)(\mu^+ - \mu^-) \arg(x_t - \zeta), \tag{14}$$

where ϕ_d is defined by (11) with $m = 2$ and x_t is the trailing edge. In this section we denote by $\arg(x_1/x_2)$ with $x_1, x_2 \in \mathbb{R}^2$ the real value of the usual function defined by the complex numbers corresponding to x_1 and x_2. The doublet strength along S follows from (12). So far we have not said anything about μ^+ and μ^-, but we still have to satisfy the Kutta condition. In the present paper we only consider aerofoils with nonzero trailing edge angle. For these cases the Kutta condition states that the flow speed must be zero at both sides of the trailing edge. Let ζ^+ and ζ^- be points at the upper and lower part of the trailing edge. The Kutta condition is satisfied if

$$D\mu(\zeta^+) \to 0 \quad \text{for} \quad |\zeta^+ - x_t| \to 0, \qquad D\mu(\zeta^-) \to 0 \quad \text{for} \quad |\zeta^- - x_t| \to 0, \tag{15}$$

where D denotes differentiation in the tangential direction. Application of conditions (12) and (15) to Eq. (14) yields the following integral equation:

$$(I - K)\mu + \beta(\mu^+ - \mu^-) = g, \tag{16}$$

with

$$K\mu(\zeta) = \frac{-1}{\pi} \int_S \mu(x) \frac{\cos(n_x, x - \zeta)}{|x - \zeta|} dS, \qquad \beta(\zeta) = \frac{1}{\pi} \arg(x_t - \zeta),$$
$$g(\zeta) = -2\mathscr{U} \cdot \zeta. \tag{17}$$

Numerical Approach

The contour S is divided into N segments S_i such that $S = \bigcup_{i=1}^N S_i$ and $S_i \cap S_j = \emptyset$, $i \neq j$. The beginning and endpoint of the ith segment are x_{i-1} and x_i

and are called nodal points. On this grid μ is approximated by a piecewise constant function μ_N and the resulting equation is solved by a collocation method. The collocation points ζ_i, $i = 1, 2, ..., N$, are taken to be the midpoints of the segments S_i. By means of projection at the collocation points we get N equations. We have, however, $N+2$ unknowns $\mu_{N,1}$, $\mu_{N,2}, ..., \mu_{N,N}$, μ_N^+, and μ_N^- with $\mu_{N,i} = \mu_N(\zeta_i)$ and $\mu_N^\pm = \mu_N(\zeta; \zeta \in S^\pm)$, so that we need two extra equations. Following condition (15) we replace μ_N^+ and μ_N^- by $\mu_{N,N}$ and $\mu_{N,1}$, i.e.,

$$\mu_N^+ = \mu_N(\zeta_N), \qquad \mu_N^- = \mu_N(\zeta_1), \tag{18}$$

where ζ_1 and ζ_N are the collocation points which are closest to the trailing edge at the lower and upper part of S. Let T_N be the projection operator defined by piecewise constant interpolation at the collocation points. We have to solve the following equation:

$$(I - T_N K)\,\mu_N + T_N \beta(\mu_{N,N} - \mu_{N,1}) = T_N g. \tag{19}$$

In aerodynamics the above numerical approach is called a first-order panel method. In [5] we have put it in a functional analytic framework. Assuming the contour S to be sufficiently smooth (except for a small region near the trailing edge) it was shown that a once continuously differentiable numerical solution can be obtained by a single iteration

$$\tilde{\mu}_N = g - (\mu_{N,N} - \mu_{N,1})\,\beta + K\mu_N. \tag{20}$$

Furthermore, it was proven that the operator K is compact on the space of essentially bounded functions, provided the boundary is sufficiently smooth. Since aerofoils (inclusive of the trailing edge) are not smooth, this property of K does not hold for our application.

Multigrid Method

The principal aim of this section is to show that Eq. (19) can be solved efficiently by a multigrid iterative process. In [2] we introduced multigrid methods for integral Eq. (1). The Jacobi relaxation was used to smooth the high-frequency errors. Assuming the integral operator to be compact, we were able to prove that the reduction factors of these multigrid methods decrease as N increases. For our application this nice property is completely destroyed (see Table I) because K is not compact. Problems with respect to the convergence of the iterative process arise in the neighbourhood of the trailing edge. Here the high-frequency errors are not removed by the Jacobi relaxation

$$\mu_N^{(\nu+1)} = T_N g + T_N K \mu_N^{(\nu)} - T_N \beta(\mu_{N,N}^{(\nu)} - \mu_{N,1}^{(\nu)}). \tag{21}$$

Inspection of the matrix corresponding to $T_N K T_N$ reveals that the cross-diagonal contains elements of magnitude $1 - k + O(1/N)$ as $N \to \infty$ with $k =$ (exterior trailing edge angle)$/\pi$. This occurrence of off-diagonal elements of about the same size as

TABLE I

Number of Iterations

Test case	τ	$N=64$			$N=128$			$N=256$		
		J	PJ	PGS	J	PJ	PGS	J	PJ	PGS
I	0	15	4	3	13	3	2	11	3	2
	$\pi/2$	15	9	9	4	7	5	2	4	2
II	0	15	8	8	13	5	5	11	3	2
	$\pi/2$	15	10	9	9	7	6	6	4	2
III	0	>25	4	3	>25	3	3	>25	3	2
	$\pi/2$	>25	12	9	19	9	6	9	6	3
IV	0	>25	11	8	>25	7	4	>25	6	4
	$\pi/2$	>25	13	10	>25	10	8	>25	7	3

Note. J, Jacobi; PJ, Paired Jacobi; PGS, Paired Gauss–Seidel.

diagonal elements explains why Jacobi relaxation does not work well. Therefore we apply another relaxation scheme, which we call *paired Gauss–Seidel relaxation.* In order to explain this scheme we first rewrite (21) as

$$\mu_{N,i}^{(\nu+1)} = g_i + \sum_{l=1}^{N} k_{il}\mu_{N,l}^{(\nu)} - \beta_i(\mu_{N,N}^{(\nu)} - \mu_{N,1}^{(\nu)}) \qquad \text{for} \quad i = 1,\ldots, N.$$

We obtain the *paired Jacobi relaxation* (PJ) scheme by removing the cross-diagonal to the left-hand side

$$\mu_{N,i}^{(\nu+1)} - k_{ij}\mu_{N,j}^{(\nu+1)} = g_i + \sum_{\substack{l=1 \\ l\neq j}}^{N} k_{il}\mu_{N,l}^{(\nu)} - \beta_i(\mu_{N,N}^{(\nu)} - \mu_{N,1}^{(\nu)}),$$

for $i = 1, 2,\ldots, N/2$ and $j = N + 1 - i$. A similar expression is obtained for $i = j$. As a result we have to solve $\frac{1}{2}N$ systems of equations of dimension 2. Substituting the new values of $\mu_{N,i}$ and $\mu_{N,j}$ as soon as they are available we obtain the paired Gauss–Seidel (PGS) relaxation scheme. For $i = 1, 2,\ldots, N/2$ and $j = N + 1 - i$ we define

$$\begin{aligned} \nu_{li} &= \nu, && \text{for} \quad i \leqslant l \leqslant j, \\ &= \nu + 1, && \text{for} \quad l < i \ \text{ and } \ l > j. \end{aligned}$$

We solve simultaneously the equations

$$\mu_{N,i}^{(\nu+1)} - k_{ij}\mu_{N,j}^{(\nu+1)} = g_i + \sum_{\substack{l=1 \\ l\neq j}}^{N} k_{il}\mu_{N,l}^{(\nu_{li})} - \beta_i(\mu_{N,N}^{(\bar{\nu})} - \mu_{N,1}^{(\bar{\nu})})$$

and

$$\mu_{N,j}^{(v+1)} - k_{jl}\mu_{N,i}^{(v+1)} = g_j + \sum_{\substack{l=1 \\ l \neq i}}^{N} k_{jl}\mu_{N,l}^{(v_{jl})} - \beta_j(\mu_{N,N}^{(\bar{v})} - \mu_{N,1}^{(\bar{v})}),$$

for $i = 1, 2,..., N/2$ and $j = N + 1 - i$, with $\bar{v} = v$ for $i = 1$ and $\bar{v} = v + 1$ for $1 < i \leqslant N/2$. The matrix elements k_{ij} can be easily calculated. Let

$$\phi_{ij} = (1/\pi) \arg|(x_j - \zeta_i)/(x_{j-1} - \zeta_i)|;$$

then

$$\begin{aligned} k_{ij} &= \phi_{ij}, && \text{for} \quad i \neq j, \\ k_{ii} &= \phi_{ii} + 1, && \text{if} \quad \phi_{ii} < 0, \\ k_{ii} &= \phi_{ii} - 1, && \text{if} \quad \phi_{ii} > 0. \end{aligned}$$

Let X_p be a short notation for the space X_{N_p} of piecewise constant functions of dimension N_p. We introduce a sequence of spaces $\{X_p \mid p = 0, 1,..., l\}$ with $N_p = 32 \times 2^p$ such that $X_0 \subset X_1 \subset \cdots \subset X_l$. The corresponding projection operators are denoted by T_p. In the context of multigrid iteration the subscript p is called level.

The calculations have been performed for several Kármán–Trefftz aerofoils with thickness $\delta = 0.05$ and length $l = 1.0$. These aerofoils are obtained from the circle in the x-plane, $x = ce^{i\theta}$, by means of the mapping

$$z = f(x) = (x - x_t)^k/(x - c(\delta - i\gamma))^{k-1},$$

where γ measures the camber and k the exterior trailing edge angle and

$$c = 2l(\delta + (1 - \gamma^2)^{1/2})^{k-1}/(2(1 - \gamma^2)^{1/2})^k, \qquad x_t = c((1 - \gamma^2)^{1/2} - i\gamma).$$

Partition of the boundary on level p. Let the interval $[0, 2\pi]$ be divided into N_p uniform segments with nodal points $\{\Theta_j \mid j = 0(1) N_p\}$. The nodal and collation points in the z plane follow from $f(ce^{i\Theta_j})$ and $f(ce^{i\Theta_{j+1/2}})$, respectively, $\Theta_{j+1/2}$ being the midpoint of subinterval $[\Theta_j, \Theta_{j+1}]$. The collocation points defined in this way are situated at the boundary and do not coincide with the collocation points of the other levels. Therefore, the elements of the matrix $\mathscr{K}_p$, $p = 0, 1,..., l$, corresponding to T_pKT_p have to be computed for all levels. Asymptotically for $l \to \infty$, the number of kernel evaluations is $\frac{4}{3}N_l^2$, when the values are computed once and stored. We have taken the following test cases:

(I) $k = 1.90$ and $\gamma = 0$,

(II) $k = 1.90$ and $\gamma = \sin 0.05$,

(III) $k = 1.99$ and $\gamma = 0$.

(IV) $k = 1.99$ and $\gamma = \sin 0.05$.

The velocity $\mathscr{V}$ of the undisturbed flow is taken to be $(\cos \tau, \sin \tau)$ with τ the angle of incidence. For the above test cases we give numerical results for $\tau = 0$ and $\tau = \pi/2$.

Algorithm. The approximate solution of (19) is obtained by the multigrid method defined in the ALGOL-68 program given in *TEXT* 1.

```
PROC mulgrid = (INT p, σ, VEC u, g) VOID:
IF p = 0
THEN solve directly (u, g)
ELSE FOR i TO σ
     DO relax (u, g); INT n = UPB u;
        VEC residu = g − u + 𝒦_p * u − β_p * (u[n] − u[1]);
        VEC um := 0_{p−1}, gm := restrict (residu);
        mulgrid (p − 1, v, um, gm);
        u := u + interpolate (um);
        relax (u, g)
     OD
FI
```

TEXT 1. *Multigrid Algorithm*

For reasons of efficiency, the number of coarse grid corrections (integer v) must be less than 4. For $v = 1$ and $v = 2$ we obtain the so-called V- and W-cycle, respectively. Here we choose $v = 2$. For the 3-D problem of flow around an ellipsoid we take $v = 1$. The interaction between the grids is defined by the procedures *restrict* and *interpolate* which are specified as follows: Let n be the upper bound of VEC u, then:

restrict $(u)[i] := 0.5 * (u[2 * i - 1] + u[2 * i])$, $i = 1(1)n/2$,
interpolate $(u)[2 * i] :=$ interpolate $(u)[2 * i - 1] := u[i]$, $i = 1(1)n$.

On level 0 the system of equations is solved by Gaussian elimination. For *relax* we take Jacobi, paired Jacobi, and paired Gauss–Seidel relaxation, respectively. We start our algorithm on level 0. The interpolation to level p $(p \geqslant 1)$ of the approximate solution from level $p - 1$ is used as the initial guess of the multigrid process at level p; truncation occurs when the residual is less than 10^{-6}. Let VEC g_p denote the restriction of g to the collocation points of level p. In ALGOL-68 notation this algorithm reads

```
solve directly (u_0, g_0);
FOR p TO 3
DO   u_p := interpolate (u_0);
     FOR i TO 25 WHILE residual > 10^-6
     DO mulgrid (p, 1, u_p, g_p) OD;
     u_0 := COPY u_p
OD;
```

TEXT 2. Implementation of the Full Multigrid Algorithm

In Table I we compare the performance of the multigrid processes using various relaxation schemes. From this table we conclude that the multigrid method defined by Jacobi relaxation is *not* acceptable (it converges too slowly). The process defined by PGS relaxation turns out to be the most efficient. Furthermore, we draw the following conclusions:

(1) the number of iterations decreases as N increases and

(2) on the highest level ($N = 256$) only a few iterations are necessary.

Calculation of Potential Flow around an Ellipsoid

The numerical approach to finding the solution of (13) is connected with the shape of the kernel function. Application of the collocation method in the space of piecewise constant functions leads to moment integrals, which consist of the calculation of solid angles. We consider the ellipsoid defined by

$$\tfrac{1}{4}x^2 + y^2 + z^2 = 1.$$

The velocity of the undisturbed flow is given by $\mathscr{V} = (1, 0, 0)$. The partition of the ellipsoid into panels is carried out as follows: First we divide the surface into N rings by planes orthogonal to the z-axis. Next each ring is divided into N^* trapeziform segments. The spherical caps are divided into N^* triangle-shaped segments. We denote these segments by S_{ij}, $i = 1,..., N$ and $j = 1,..., N^*$. The collocation points are chosen to be the "midpoints" of these segments and are situated at the surface. The solid angle subtended at ζ by S_{ij} with $\zeta \notin S_{ij}$ is given by

$$\int_{S_{ij}} \frac{\cos(n_x,\ x - \zeta)}{|x - \zeta|^2}\, dS_x.$$

In contrast with 2-D, in general these integrals cannot be evaluated analytically. We approximate S_{ij} by one or two flat planes. The solid angles subtended by such planes *can* be evaluated analytically.

Multigrid Method

The different grids are related by $N_p = 4 \times 2^p$ and $N_p^* = 4 \times 2^p$. Putting $\beta_p = 0$, we use the algorithm given in *TEXT* 1 with $\nu = 1$. Analogously to 2-D we define the procedures "solve directly," "restrict," and "interpolate" by Gaussian elimination, weighted injection, and piecewise constant interpolation, respectively. For "relax" we take the Jacobi relaxation scheme. Assuming the surface to be smooth, Wolff [6] has analysed this multigrid method. He has proven that the reduction factor of the multigrid process is less than ch^α for $h \to 0$, where h and α are a measure for the mesh size and the smoothness of the surface, respectively. For the ellipsoid $\alpha = 1$.

TABLE II

Potential Flow around an Ellipsoid: Multigrid Method[a]

$l = 2$; $N_2 = 16$, $N_2^* = 16$			$l = 3$; $N_3 = 32$, $N_3^* = 32$		
Iter.	Residual	Red. factor	Iter.	Residual	Red. factor
1	1.17×10^{-1}		1	4.56×10^{-2}	
2	2.04×10^{-3}	4.13×10^{-2}	2	4.34×10^{-4}	1.67×10^{-2}
3	7.75×10^{-5}	1.40×10^{-2}	3	8.48×10^{-6}	6.98×10^{-3}
4	1.89×10^{-6}	4.63×10^{-2}	4	9.93×10^{-8}	2.56×10^{-2}
5	6.54×10^{-8}	2.36×10^{-2}			
	Mean red. factor: 2.83×10^{-2}			Mean red. factor: 1.44×10^{-2}	
	Operation count: 10.68			Operation count: 8.53	

Note. The ellipsoid is given by $\frac{1}{4}x^2 + y^2 + z^2 = 1$; $\mathscr{H}$ is parallel to the x axis.
[a] $N_0 = 4$, $N_0^* = 4$.

Numerical Results

In Tables II and III, we give the residuals and the observed reduction factors

$$\eta_i = \| \mu_N^{(i+1)} - \mu_N^{(i)} \| / \| \mu_N^{(i)} - \mu_N^{(i-1)} \|,$$

with $\| \cdot \|$ the supremum norm. We also give the mean reduction factor

$$\bar{\eta} = \left\{ \prod_{i=1}^{k} \eta_i \right\}^{1/k}$$

TABLE III

Potential Flow around an Ellipsoid: Jacobi Iterative Process

$N = 16$, $N^* = 16$			$N = 32$, $N^* = 32$		
Iter.	Residual	Red. factor	Iter.	Residual	Red. factor
1	1.73		1	2.15	
2	8.05×10^{-1}	4.51×10^{-1}	2	1.20	5.44×10^{-1}
3	3.82×10^{-1}	4.68×10^{-1}	3	6.72×10^{-1}	5.57×10^{-1}
4	1.83×10^{-1}	4.75×10^{-1}	4	3.79×10^{-1}	5.62×10^{-1}
5	8.75×10^{-2}	4.78×10^{-1}	5	2.14×10^{-1}	5.64×10^{-1}
6	4.20×10^{-2}	4.79×10^{-1}	6	1.21×10^{-1}	5.65×10^{-1}
7	2.01×10^{-2}	4.80×10^{-1}	7	6.85×10^{-2}	5.65×10^{-1}
			8	3.88×10^{-2}	5.66×10^{-1}
⋮	⋮	⋮	⋮	⋮	⋮
21	6.94×10^{-7}	4.80×10^{-1}	27	7.79×10^{-7}	5.66×10^{-1}
	Mean red. factor: 4.77×10^{-1}			Mean red. factor: 5.64×10^{-1}	
	Operation count: 21			Operation count: 27	

Note. The ellipsoid is given by $\frac{1}{4}x^2 + y^2 + z^2 = 1$; $\mathscr{H}$ is parallel to the x axis.

and the operation count expressed in work units. One work unit is defined by (total number of multiplications)/$(N_l \times N_l^*)^2$ with l the highest level. We only take into account matrix–vector multiplications and the direct solution on the coarsest grid for which we count $\frac{1}{3}(N_0 \times N_0^*)^3$ multiplications. Tables II and III enable us to draw the following conclusions:

(1) Comparing the results obtained with $l = 2$ and $l = 3$ we see that the mean reduction factor of the multigrid method has been decreased by a factor of 2, which is in agreement with the theoretical results of Wolff [6] and

(2) the multigrid method is much cheaper than the Jacobi iterative process.

Calculation of Oscillating Disk Flow

The rotating flow due to an infinite disk performing torsional oscillations at an angular velocity $\Omega \sin \omega\tau$ in a viscous fluid otherwise at rest involves two relevant length scales, (1) the Von Kármán layer thickness $(\nu/\Omega)^{1/2}$, where ν is the kinematic viscosity and (2) the Stokes layer thickness $(\nu/\omega)^{1/2}$. By means of the Von Kármán similarity transformations, the velocities (u, v, w) in a cylindrical coordinate system (r, ϕ, x) can be written as

$$u = \Omega r f(z, t), \qquad v = \Omega r g(z, t), \qquad w = -2(2\nu\omega)^{1/2} h(z, t),$$

where $z = (\Omega^2/2\nu\omega)^{1/2} x$ and $t = \omega\tau$. In that case the Navier–Stokes equations reduce to partial differential equations (2)–(4). Apparently the oscillating disk flow is characterized by the parameter $\varepsilon = \Omega/\omega$, which determines the ratio of the Stokes layer thickness to the Von Kármán layer thickness.

For the high-frequency flow ($\varepsilon \ll 1$) analytical solutions are found in the literature in the form of series expansions in terms of ε. This type of flow consists of an oscillatory inner layer (i.e., Stokes layer) near the rotating disk and a secondary outer layer (i.e., Von Kármán layer). Using a multiple scaling technique, Benney [7] was able to find series expansions valid throughout the region of flow. The first-order terms of the solution are given by

$$g(z, t) = e^{-z/\varepsilon} \sin(t - z/\varepsilon), \qquad f(z, t) \sim \varepsilon e^{-4az} \qquad \text{for} \quad z \to \infty, \tag{22}$$

with $a = 0.265$. In [3] we used this technique to determine the axial inflow at infinity up to the term with ε^3

$$h(\infty, 0) = a\varepsilon + \{ab + \tfrac{1}{16}(\sqrt{2} - 1)\}\, \varepsilon^2 + O(\varepsilon^3), \tag{23}$$

with $b = -0.207$. Inspection of (22) reveals that problem (2)–(6) is singularly perturbed and for a fixed t the solution contains more and more high frequency components as $\varepsilon \to 0$.

In this paper we discuss two computational methods to find the periodic solution satisfying (6). The first method is based on simulation of the physical process by taking the state of rest as an initial condition and eliminating the transient effects by integration in time. In mathematical terminology this process can be interpreted as Picard's method for computing a fixed point. Let the velocity vector be

$$v = (f, g, h).$$

Denote by $(v(z, t); v_0)$ the solution of the usual initial value problem (2)–(5) with initial data

$$v(z, 0) = v_0(z). \tag{24}$$

Assume that the initial data v_0 belong to a suitable class $\mathscr{L}$. Define a map of $\mathscr{L}$ into itself by the equation

$$K_\varepsilon(v_0) := (v(\cdot, 2\pi); v_0), \tag{25}$$

being the solution of (2)–(5) and (24) at $t = 2\pi$. Since (2)–(4) is a parabolic system, K_ε may be expected to have a smoothing influence, just as the integral operators of the Fredholm equations studied in [2]. In operator notation simulation of the physical process is written as the Picard sequence

$$v_{i+1} = K_\varepsilon(v_i) \qquad \text{with} \quad v_0 = 0. \tag{26}$$

Periodic condition (6) can be rewritten as

$$v = K_\varepsilon(v), \qquad v \in \mathscr{L}. \tag{27}$$

We remark that K_ε is a nonlinear operator. For $\varepsilon < 1$, (26) converges slowly. Therefore we have devised another method. Since Eq. (27) has a superficial resemblance with a Fredholm equation of the second kind, we have applied a multigrid method to (27).

Numerical Approach

This section is divided into two parts:

(1) the numerical solution of initial boundary value problem (2)–(5) with initial data (24) and

(2) numerical methods for finding periodic solutions satisfying (6).

Discretization of the Initial Boundary Value Problem

Consider partial differential equations (2)–(4) with boundary conditions (5) and initial data (24). To this problem we apply implicit finite difference techniques in combination with an appropriate stretching function for the construction of the

computational grid. In calculations the boundary conditions at infinity are applied at a finite value $z = l$

$$f(l, t) = g(l, t) = 0. \tag{28}$$

We want to resolve the flow structure near the disk with a limited number of mesh points. Therefore, taking (22) into account, we transform the z coordinate by

$$z(x) = l(\varepsilon x + (1 - \varepsilon)x^3), \qquad x \in [0, 1], \tag{29}$$

and we take the mesh covering of the new range $0 \leqslant x \leqslant 1$ uniform with step size $\Delta x = 1/N$. Integration in time is done by the Euler backward formula

$$g_t = (g_{k+1} - g_k)/\Delta t \qquad \text{with} \quad \Delta t = 2\pi/T.$$

The right-hand sides of (2) and (3) are discretized by central differences at $t = t_{k+1}$. The left- and right-hand sides of (4) are integrated by means of the midpoint and trapezoidal rule, respectively. The resulting nonlinear system of finite difference equations is solved by means of Newton iteration, which is terminated if the residual is less than 10^{-6}. For further details see [3].

Numerical Methods for Computing Periodic Solutions

Using the above finite difference approach we define the discrete counterpart of the operator K_ε and the velocity vector v by $\mathscr{K}_{\varepsilon;N,T,l}$ and v_N, respectively. In discrete operator notation the periodic condition reads

$$v_N = \mathscr{K}_{\varepsilon;N,T,l}(v_N). \tag{30}$$

In the present paper we propose two computational methods to solve (30):

(A) simulation of the physical process by Picard iteration and

(B) a multigrid method.

In the first method the parameters ε, N, T, and l are fixed. In the second method the parameters N and T are taken from a sequence $\{(N_p, T_p)\}$, $p = 0, 1, \ldots, L$ such that with $p = L$ we have $N_L = N$, $T_L = T$ and with $p < q \leqslant L$ we have $N_p \leqslant N_q$, $T_p \leqslant T_q$ (i.e., a smaller p corresponds with a coarser discretization).

(A) Simulation of the physical process. We take the state of rest ($v_N^{(0)} \equiv 0$) as an initial condition. The transient effects are eliminated by Picard's method

$$v_N^{(i+1)} = \mathscr{K}_{\varepsilon;N,T,l}(v_N^{(i)}). \tag{31}$$

The iteration index i counts the number of periods that are calculated. This process is truncated if the residual $\| v_N^{(i)} - \mathscr{K}_{\varepsilon;N,T,l}(v_N^{(i)}) \|$ is less than 0.5×10^{-4}. Here

$$\| v_N \| = \max_{0 \leqslant j \leqslant N} |g_j| + \max_{0 \leqslant j \leqslant N} |h_j|.$$

(B) Multigrid method. We introduce a sequence of grids with $N_p = 20 \times 2^p$ and $T_p = 8 \times 2^p$. The integer p is called the level. We replace the subscript N_p by p,

$$v_{N_p} = v_p \qquad \text{and} \qquad \mathscr{H}_{\varepsilon;N_p,T_p,l} = \mathscr{H}_{\varepsilon;p}.$$

Denote the velocity at grid point x_j on level p by $v_p[j] = (f_j, g_j, h_j)$. The addition $v_p[j] + v_p[k]$ and the multiplication $c \times v_p[j]$ are defined as usual (element by element). The interaction between the grids is defined by piecewise-linear interpolation

$$\begin{aligned} &\text{interpolate}(\mathscr{U})[j] \\ &\quad = \mathscr{U}[j/2], && j = 0, 2, \ldots, 2N, \\ &\quad = 0.5 \times (\mathscr{U}[(j+1)/2] + \mathscr{U}[(j-1)/2]), && j = 1, 3, \ldots, 2N-1, \end{aligned}$$

and by injection

$$\text{restrict}(\mathscr{U})[j] = \mathscr{U}[2j], \qquad j = 0, 1, \ldots, N/2,$$

where N is the upper bound of the velocity vector $\mathscr{U}$.

We use a multigrid method that starts on level 0 with simulation of the phsyical process (method A). For small values of ε we apply continuation. Suppose we have the following ε-sequence $\{\varepsilon_l \mid \varepsilon_0 > \varepsilon_1 > \cdots > \varepsilon_m$ with $\varepsilon_0 = 1\}$. At each stage of this continuation process we approximately solve the equation $v_0 = \mathscr{H}_{\varepsilon_l;0}(v_0)$ by (31) until the residual is less than 0.5×10^{-3}. As the initial guess of (31) we take the solution of the previous stage ($\varepsilon = \varepsilon_{l-1}$). For $\varepsilon = \varepsilon_0$ we take the state of rest. Denote the solution of this continuation method by $v_0(\varepsilon_0, \varepsilon_1, \ldots, \varepsilon_m)$.

Since (30) is a nonlinear equation, it is only solved approximately. Let $\mathscr{U}_p$ be an approximation to the solution v_p of (30) on level p. We define the defect of $\mathscr{U}_p$ by

$$\mathscr{d}_p = \mathscr{U}_p - \mathscr{H}_{\varepsilon;p}(\mathscr{U}_p).$$

The multigrid method is given by the ALGOL-68 program in TEXT 3, where VELO is a mode for the vector of unknowns:

```
MODE VELO = STRUCT(VEC f, g, h).
PROC compute periodic solution = (# to level # INT l) VOID:
(U_0 := v_0(ε_0, ε_1, ..., ε_m).
FOR j TO l
DO   d_{j-1} := U_{j-1} - H_{ε;j-1}(U_{j-1});
     U_j := interpolate(U_{j-1});
     multigrid(j, 1, U_j, 0_j)
OD
);
PROC multigrid = (INT m, σ, REF VELO U, VELO y) VOID:
(IF m = 0
```

```
THEN FOR k TO 50 WHILE residual > δ_ε
      DO VELO r = y − 𝒰 + 𝒦_{ε;m}(𝒰);
          residual := ‖ r ‖;
          𝒰 := 𝒰 + ω_k * r
      OD
ELSE FOR i TO σ
      DO 𝒰 := y + 𝒦_{ε;m}(𝒰);
          VELO d = d_{m−1} − restrict(y − 𝒰 + 𝒦_{ε;m}(𝒰));
          VELO v := COPY 𝒰_{m−1};
          multigrid(m − 1, 2, v, d);
          𝒰 := 𝒰 + interpolate(𝒰_{m−1} − v)
      OD
FI
);
```

TEXT 3. Multigrid Algorithm for the Computation of Periodic Solutions of Parabolic Equations

The structure of this multigrid algorithm has been proposed by Hackbusch [8] for the numerical solution of general time-periodic parabolic problems. Here we apply it to the particular problem of oscillating disk flow.

On level 0 of "multigrid" we use overrelaxation for extremely small values of ε. The parameter ω_k takes the values 1, 2, and 4. Initially we put $\omega_k = 1$. If the axial inflow converges slowly it is multiplied by a factor of 2. As soon as the residual increases, the value $\omega_k = 1$ is restored.

Numerical Results

From Zandbergen and Dijkstra [9] it is known that Von Kármán's rotating disk solution can be represented sufficiently accurate with $l = 12$; hence we fix infinity at this value. We give numerical results for the following values of ε:

$$\varepsilon_0 = 1, \qquad \varepsilon_1 = 0.5, \qquad \varepsilon_2 = 0.1, \qquad \varepsilon_3 = 0.05.$$

This sequence is also applied in the continuation process that is used to find an approximation $\mathscr{U}_0$ of the multigrid method, e.g., for $\varepsilon = 0.1$ we have $\mathscr{U}_0 := v_0(1, 0.5, 0.1)$. For $N = 160$ and $T = 64$ we compare the performance of simulation of the physical process (method A) and the multigrid method (B). On the coarsest grid the latter method needs 20 step sizes in space and 8 step sizes in time; hence it uses four levels: 0, 1, 2, and 3.

Let a work unit be defined by the computational work needed for calculating one Picard iterate with $N = 160$ and $T = 64$. In Table IV we compare the computed axial inflow at infinity with the value of its asymptotic approximation (23) for $\varepsilon \to 0$. Between parentheses we give the number of work units and the iteration error $\| \mathscr{U}_N - \mathscr{K}_{\varepsilon;N,T,l}(\mathscr{U}_N) \|$, where $\mathscr{U}_N$ is the final solution.

TABLE IV

Axial Inflow

ε	Method A	Method B	(23)
1.0	0.2014 $(8, 4.4 \times 10^{-5})$	0.2014 $(6.8, 9.3 \times 10^{-7})$	0.2360
0.5	0.1177 $(17, 4.7 \times 10^{-5})$	0.1178 $(7.0, 3.9 \times 10^{-6})$	0.1253
0.1	0.0236 $(74, 4.9 \times 10^{-5})$	0.0271 $(7.4, 1.6 \times 10^{-5})$	0.0262
0.05	0.0083 $(72, 4.9 \times 10^{-5})$	0.0137 $(12.5, 3.3 \times 10^{-6})$	0.0132

Note. Between parentheses are the number of work units and the residual.

On level 0 of the multigrid method we used Picard iteration (i.e., $\omega_k \equiv 1$) for $\varepsilon \geqslant 0.1$. The iterative process was terminated when the residual was less than $\delta_\varepsilon = 0.5 \times 10^{-4}$. For $\varepsilon = 0.05$ we have applied overrelaxation ($1 \leqslant \omega_k \leqslant 4$) and we have put $\delta_{0.05} = 10^{-7}$. That is the reason why the computational work increased for this case.

From Table IV we conclude that the multigrid method becomes more efficient as ε decreases. For $\varepsilon = 0.1$ the computational work has been reduced by a factor of 10. For $\varepsilon = 0.1$ and $\varepsilon = 0.05$ the numerical results of method A still contain a low-frequency error. In this case the test for termination of the physical process is not adequate. The process converges slowly, as can be seen from Fig. 1, in which we have

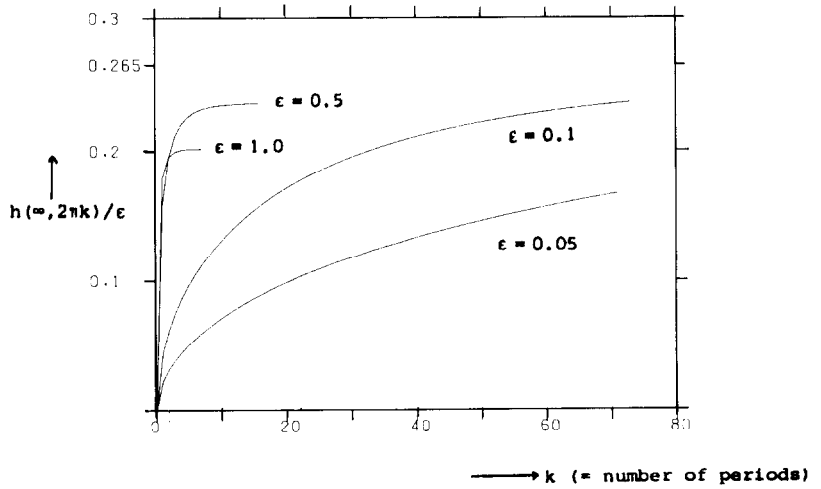

FIG. 1. Dependence of the axial inflow on the number of periods.

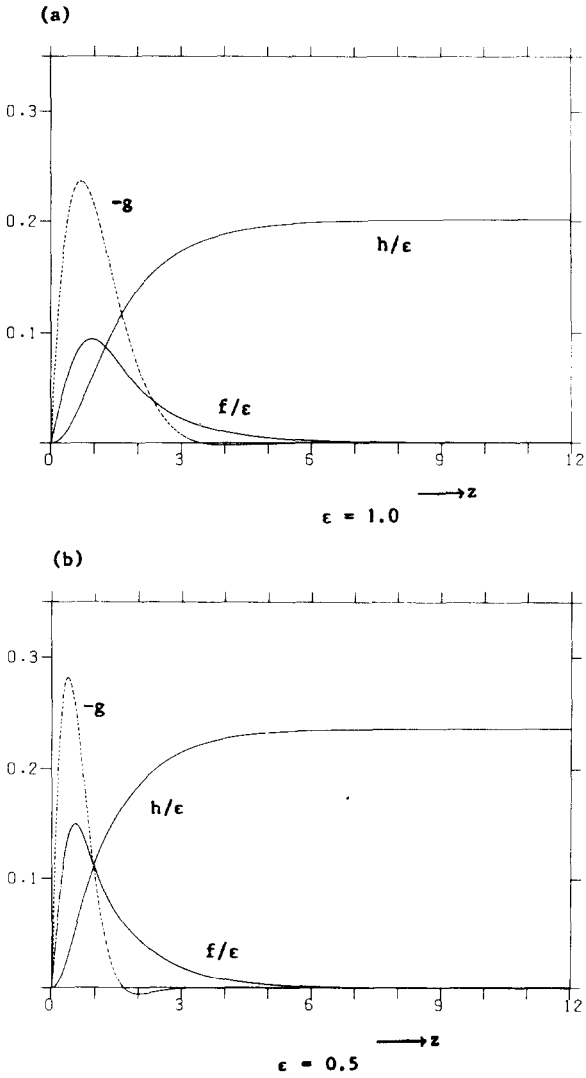

FIG. 2. Velocity profiles.

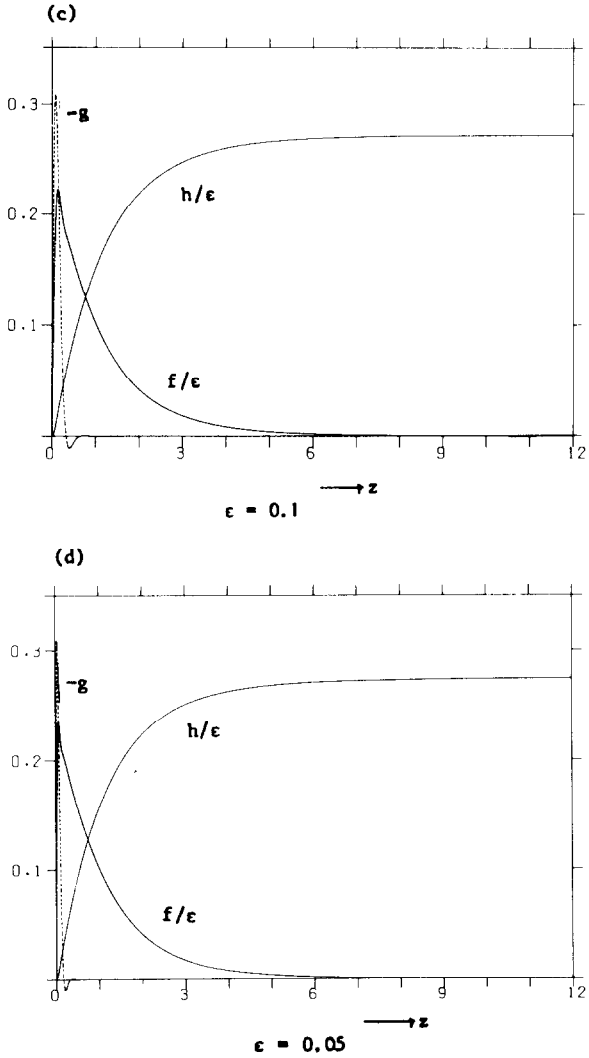

FIGURE 2 *(continued)*

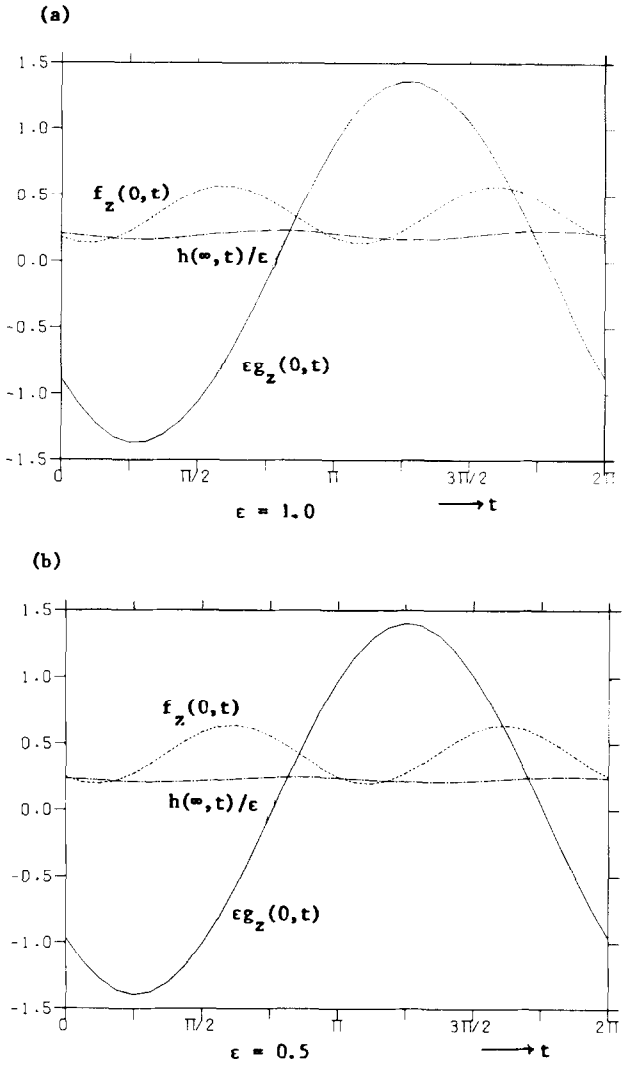

FIG. 3. Axial inflow and shear stresses.

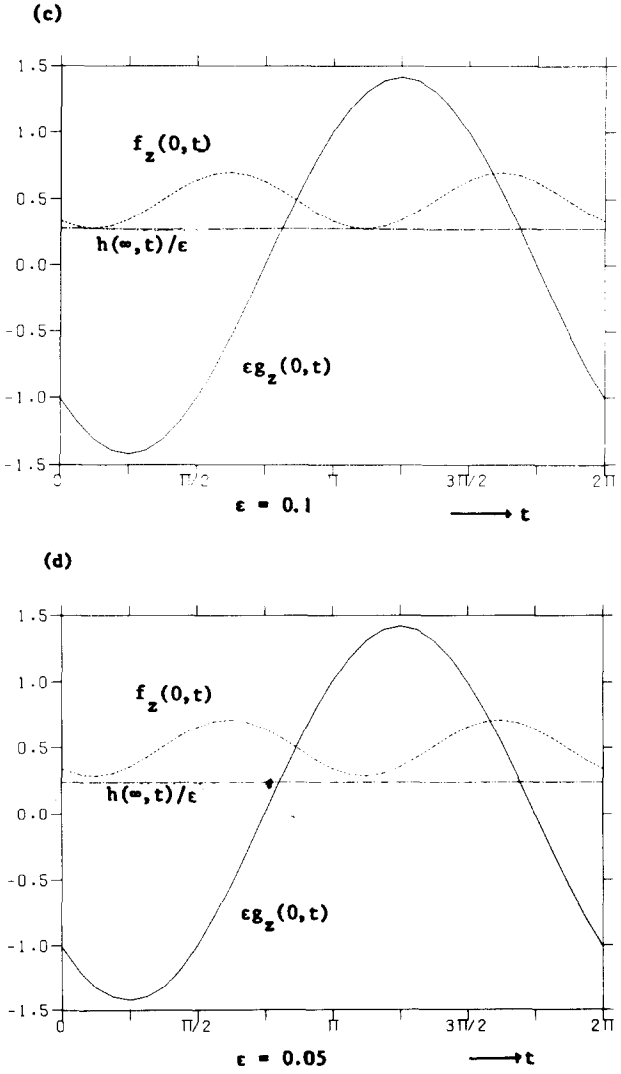

FIGURE 3 *(continued)*

displayed the axial inflow as a function of the number of periods. For $\varepsilon = 0.05$ the axial inflow is still increasing after 72 periods. The same phenomenon occurs on the coarsest grid of the multigrid method. Therefore we have applied overrelaxation.

The results of our analysis are given in Figs. 2 and 3. The profiles of the variables f/ε, g, and h/ε are displayed in Fig. 2. We see that there is an oscillatory boundary layer. For smaller values of ε (see Figs. 2c and d) the azimuthal component of velocity (g) is confined to this boundary layer and the radial and axial component of velocity (resp. f and h) persist outside this layer. The results for the quantities $\varepsilon g_z(0, t)$, $f_z(0, t)$ and $h(\infty, t)/\varepsilon$ are displayed in Fig. 3. Comparing these figures we see that the fluctuations in $h(\infty, t)$ decrease as $\varepsilon \to 0$. This means that outside the boundary layer the fluid motion becomes stationary (i.e., the outer flow does not depend on t). These numerical results are in agreement with the analytical solutions of Benney [7].

Finally, from the results just presented we conclude that for the computation of periodic solutions of the single disk problem for $\varepsilon \leqslant 1$, the multigrid method is preferable, whereas for $\varepsilon > 1$ simulation of the physical process may be employed.

ACKNOWLEDGMENT

This paper is based on parts of the Doctor's Thesis of the author prepared under the guidance of Professor P. Wesseling of Delft University of Technology.

REFERENCES

1. A. BRANDT, *Math. Comput.* **31**(138) (1977), 333.
2. P. W. HEMKER AND H. SCHIPPERS, *Math. Comput.* **36**(153) (1981), 215.
3. H. SCHIPPERS, *J. Eng. Math.* **13**(2) (1979), 173.
4. N. I. MUSCHELISCHWILI, "Singuläre Integralgleichungen," Akademie-Verlag, Berlin, 1965.
5. H. SCHIPPERS, *J. Eng. Math.* **16**(1) (1982), 59.
6. H. WOLFF, "Multigrid Method or the Calculation of Potential Flow around 3-D Bodies," Report NW 119/82, Mathematisch Centrum, Amsterdam, 1982, preprint.
7. D. J. BENNEY, *J. Fluid Mech.* **18**(3) (1964), 385.
8. W. HACKBUSCH, *SIAM J. Sci. Stat. Comput.* **2**(2) (1981), 198.
9. P. J. ZANDBERGEN AND D. DIJKSTRA, *J. Eng. Math.* **11**(2) (1977), 167.